

Energy-Transfer Process in Crystals of Chiral and Racemic Double Complex Salts of $[Co(ethylenediamine)_3][Tb(2,6\text{-}pyridinedicarboxylate)_3]$

Munetaka Iwamura,* Toshiaki Tsukuda, and Makoto Morita

Department of Applied Chemistry, Seikei University, Kichijoji, Musashino, Tokyo 180-8633

Received October 30, 2006; E-mail: miwamura@riken.jp

Luminescence and energy-transfer reactions in double complex crystals of $[Co(en)_3][Tb(dpa)_3]$ (en = ethylenediamine, dpa = 2,6-pyridinedicarboxylate) were investigated and compared to single crystals of *rac*-$[Co(en)_3]$·*rac*-$[Tb(dpa)_3]$ (double complexes salt of racemic $[Co(en)_3]^{3+}$ and racemic $[Tb(dpa)_3]^{3-}$) and Δ-$[Co(en)_3]$·*rac*-$[Tb(dpa)_3]$ (chiral $[Co(en)_3]^{3+}$ and racemic $[Tb(dpa)_3]^{3-}$ salt). The energy-transfer rate constants from Tb^{3+} to Co^{3+} complexes were determined from the time profile of emission intensity of photo-excited Tb^{III} ion in the double complex crystals. The emission decay profiles of *rac*-$[Co(en)_3]$·*rac*-$[Tb(dpa)_3]$ were analyzed with single exponential curves. On the other hand, the profiles of Δ-$[Co(en)_3]$·*rac*-$[Tb(dpa)_3]$ show double-exponential curves. From the X-ray analysis of crystal structures, it was found that there is only one site for $[Tb(dpa)_3]^{3-}$ in *rac*-$[Co(en)_3]$·*rac*-$[Tb(dpa)_3]$ crystal, and there are two sites in the Δ-$[Co(en)_3]$·*rac*-$[Tb(dpa)_3]$ crystal, i.e., Δ-$[Tb(dpa)_3]^{3-}$ and Λ-$[Tb(dpa)_3]^{3-}$ are put in different sites in the crystal. The two rate constants obtained from the double-exponential curve of Δ-$[Co(en)_3]$·*rac*-$[Tb(dpa)_3]$ are assigned to energy-transfer rates from Δ-$[Tb(dpa)_3]^{3-}$ and Λ-$[Tb(dpa)_3]^{3-}$ in the crystal. A distance dependence was determined from the obtained energy-transfer rate constants and the Tb–Co distances in the crystals according to a Dexter type electron-exchange mechanism of energy-transfer model. The energy-transfer rate constants in the crystals are comparable in magnitude with energy-transfer rates in quenching experiments in the $[Tb(dpa)_3]^{3-}$–$[Co(en)_3]^{3+}$ aqueous solution.

The electronic energy-transfer reactions between metal complexes are very important in the fields of solar energy, practical luminescence, and basic research of molecular interactions in condensed phase.[1–3] They depend on spectral overlap, distance, and relative orientation between donors and acceptors. To know the exact details of the energy transfer in the condensed phase would be of great benefit to not only the field of energy transfer but also that of electron-transfer reactions or other chemical reactions in the media.

Energy-transfer reactions from photo-excited $[Tb(dpa)_3]^{3-}$ (dpa = 2,6-pyridinedicarboxylate) to Co^{III} complexes are very interesting, because the reaction rate constants are very sensitive to small change in the relative position (distance and/or orientation) between Tb^{III} ion and Co^{III} ion in the reaction systems. For the energy-transfer reaction of $[Tb(dpa)_3]^{3-}$ to $[Co(en)_3]^{3+}$ (en = ethylenediamine), Metcalf et al. have reported the enantio-selective quenching process in solution.[4] The circularly polarized luminescence reflects the difference in the energy-transfer rate from Δ-$[Tb(dpa)_3]^{3-}$ to Δ-$[Co(en)_3]^{3+}$ and Λ-$[Tb(dpa)_3]^{3-}$ to Δ-$[Co(en)_3]^{3+}$. It indicates that distance, and/or relative orientation between $[Tb(dpa)_3]^{3-}$ and $[Co(en)_3]^{3+}$ are different between encounter complexes of homo (Δ–Δ) and hetero (Λ–Δ) pairs in solution. More recently, we have reported the specific ion effects on energy-transfer reactions between metal complexes in aqueous solutions.[5–8] For example, rate constants of energy-transfer reaction of $[Td(dpa)_3]^{3-}$ to $[Co(bpy)_3]^{3+}$ (bpy = bipyridine) and $[Co(en)_3]^{3+}$ in aqueous solutions are affected by coexisting anions in the order of $ClO_4^- > Br^- \approx Cl^-$ for $[Tb(dpa)_3]^{3-}$–$[Co(en)_3]^{3+}$.[8] In these studies, it has been concluded that coexisting ion dependence of the energy-transfer rates are due to the variation of the distances between the donors and acceptors in encounter complexes induced by the coexisting ions.

However, the distances or relative orientations between the reactants in the encounter complexes in solution has not been discussed in these papers. Thus, it is very significant to compare the energy-transfer rate in aqueous solutions and in media, where distances between donor and acceptor molecules can be determined. We can see the exact distance and orientation between donor and acceptor from X-ray analysis of single crystals. Observations and studies of direct energy-transfer reactions from donor species to neighboring acceptors in single crystals have been performed for crystals of double metal complexes, which are composite of energy donor and acceptor complexes with their X-ray crystal analysis.[1,9–11] For example, Otsuka et al. have reported the studies concerning energy-transfer reactions in double crystals of polypyridine $[Ru(N\text{-}N)_3]^{2+}$ (N-N = bpy, phenanthroline) and $[Cr(CN)_6]^{3-}$.[9] They have shown that there is a dependence of the energy-transfer reaction on the relative orientation between donor and acceptor. Brayshaw et al. have studied double crystals of $[RE(dpa)_3]^{3-}$ (RE = Tb, Eu, and Gd) and Cr^{III} and Co^{III} complexes.[11] They have assigned the energy-transfer reaction from $[RE(dpa)_3]^{3-}$ to Cr^{III} complexes and their rate constants. They have reported a crystal structure of $[Co(sar)][Eu(dpa)_3]$ (sar = sarcophagine), but not of $[M(en)_3][RE(dpa)_3]$.

Published on the web June 13, 2007; doi:10.1246/bcsj.80.1140

In present study, energy transfer from $[Tb(dpa)_3]^{3-}$ to $[Co(en)_3]^{3+}$ in single crystals composite from these complexes were investigated. Single crystals of double complex salts of chiral and racemic $[Co(en)_3]^{3+}$ and $[Tb(dpa)_3]^{3-}$, Δ-$[Co(en)_3]$·*rac*-$[Tb(dpa)_3]$, *rac*-$[Co(en)_3]$·*rac*-$[Tb(dpa)_3]$ were synthesized, and their crystal structures are reported. Energy transfers in Δ-$[Co(en)_3]$·*rac*-$[Tb(dpa)_3]$ and *rac*-$[Co(en)_3]$·*rac*-$[Tb(dpa)_3]$, of which the emission and absorption spectra are quite identical, are compared. The energy-transfer rate constants were estimated from these samples as a function of accurate inter-atomic distance between Tb–Co taken from the X-ray crystal structures of these double complex crystals according to electron-exchange energy-transfer mechanism. The values of energy-transfer rates are comparable with Tb–Co energy-transfer rates in aqueous solution determined previously. Thus, the distance between donor and acceptor in the encounter complexes in solutions were estimated from obtained distance dependence of the energy-transfer reaction in $[Co(en)_3][Tb(dpa)_3]$ crystals.

Experiment

Preparation of Double Complex Crystals. Preparation of $K_3[Tb(dpa)_3]$ has been described elsewhere.[6] Δ-$[Co(en)_3]$Cl·L-tart (tart = tartaric acid) and *rac*-$[Co(en)_3]Cl_3$ were prepared by method in literatures.[12]

Large single crystals of $[Co(en)_3][Tb(dpa)_3]$ were not obtained by simple evaporation of solvents of solution due to their low solubility. Therefore, following method was used. A concentrated aqueous solution of $K_3[Tb(dpa)_3]$ was poured into one side of U-shaped glass tube, which is half filled with agar in a 1:20 ratio with water, and a concentrated aqueous solution of Δ-$[Co(en)_3]$Cl·L-tart was added to the other side. After about one week, plate shaped orange crystals of Δ-$[Co(en)_3]$·*rac*-$[Tb(dpa)_3]$ about 1 mm in size were generated in the agar.

Single crystals of *rac*-$[Co(en)_3]$·*rac*-$[Tb(dpa)_3]$ were also obtained by the above method by using *rac*-$[Co(en)_3]Cl_3$ instead of Δ-$[Co(en)_3]$Cl·L-tart.

Measurements. Luminescence spectra were measured with excitation of a N_2 laser (337 nm, Spectra-Physics 337) using a computer-controlled spectroscopic system based on a Spex 1401 double monochromator and SR400 photon counter. Luminescence decay at 546 nm of $[Tb(dpa)_3]^{3-}$ was measured following repeated short excitation pulses with the N_2 laser. The time profile of the emission was recorded with a TDS550 digital oscilloscope. The time resolution for this system was ca. 10 ns, which was checked by measuring well known samples, e.g., $[Ru(bpy)_3]^{2+}$ aqueous solution. The temperature of the samples was controlled with an Air Products closed cycle He Cryostat.

Solid samples were held by binding to quartz cover glass plates. In the temperature-dependence measurements, samples were held on the copper plate with paste. The racemic crystal *rac*-$[Co(en)_3]$·*rac*-$[Tb(dpa)_3]$ was immersed in water in binding quartz cover glass plates during measurements because the single crystal crumbles into powder in air at room temperature by losing solvent molecules, but it is stable if it is immersed in water.

Crystal Structural Determination. Single crystals of Δ-$[Co(en)_3]$·*rac*-$[Tb(dpa)_3]$ are stable in the atmosphere at room temperature. Therefore, we can obtain the accurate crystal structure by conventional method. On the other hand, single crystals of *rac*-$[Co(en)_3]$·*rac*-$[Tb(dpa)_3]$ were not stable and crumbled into powder in air at room temperature, but they were stable if they were immersed in water at room temperature or cooled to under 0 °C. Crystal structure of *rac*-$[Tb(dpa)_3]$·*rac*-$[Co(en)_3]$ was obtained by blowing 77 K N_2 gas. Data collection was performed using AFC-5S diffractometer (Rigaku) for the crystal of Δ-$[Co(en)_3]$·*rac*-$[Tb(dpa)_3]$, and Saturn 70 CCD System (Rigaku) for *rac*-$[Co(en)_3]$·*rac*-$[Tb(dpa)_3]$. The structures were solved by using direct methods (SIR-92 programs, Rigaku). The data were corrected with the Crystal Structure 3.6.0. (Rigaku) software. Crystallographic data have been deposited with Cambridge Crystallographic Data Centre: Deposition number CCDC-262808 and CCDC-262809 for *rac*-$[Co(en)_3]$·*rac*-$[Tb(dpa)_3]$ and Δ-$[Co(en)_3]$·*rac*-$[Tb(dpa)_3]$, respectively. Copies of the data can be obtained free of charge via http://www.ccdc.cam.ac.uk/conts/retrieving.html (or from the Cambridge Crystallographic Data Centre, 12, Union Road, Cambridge, CB2 1EZ, UK; Fax: +44 1223 336033; e-mail: deposit@ccdc.cam.ac.uk.

Results and Discussion

Emission Spectrum. Crystals of $K_3[Tb(dpa)_3]$, *rac*-$[Co(en)_3]$·*rac*-$[Tb(dpa)_3]$, and Δ-$[Co(en)_3]$·*rac*-$[Tb(dpa)_3]$ showed green light emissions by excitation of 337 nm of N_2 laser. In the emission spectrum, $K_3[Tb(dpa)_3]$ showed characteristic sharp peaks assigned to $^5D_4 \rightarrow {}^7F_J$ ($J = 0, 1, \ldots, 6$) of Tb^{3+} via energy transfer from the ligands, which are excited by the UV right. Figure 1 shows emission spectrum of single crystals of *rac*-$[Co(en)_3]$·*rac*-$[Tb(dpa)_3]$ and Δ-$[Co(en)_3]$·*rac*-$[Tb(dpa)_3]$. The spectra of *rac*-$[Co(en)_3]$·*rac*-$[Tb(dpa)_3]$ and Δ-$[Co(en)_3]$·*rac*-$[Tb(dpa)_3]$ were almost the same as that of $K_3[Tb(dpa)_3]$. Therefore, the emission peaks of the $[Co(en)_3]$·$[Tb(dpa)_3]$ salts were assigned to transition $^5D_4 \rightarrow {}^7F_J$ ($J = 0, 1, \ldots, 6$) of Tb^{III} ion. However, their intensities were much weaker than that of $K_3[Tb(dpa)_3]$ powder, which means the emission of Tb^{III} ion is quenched by the Co^{III} complex. Metcalf et al. proposed that the mechanism of the quenching in the $[Tb(dpa)_3]^{3-}$ to $[Co(en)_3]^{3+}$ system is the energy transfer from Tb^{3+} ion to Co^{3+} ion (Tb–Co ET), because the emission spectra of the f–f transition is overlapped by an absorption spectrum of the d–d transition of $[Co(en)_3]^{3+}$ (Fig. 1).[4,8,10,11]

Time-Resolved Emission Intensity. Emission decay rate constants of $[Co(en)_3][Tb(dpa)_3]$ crystals were about $1–3 \times 10^6\ s^{-1}$ (See below), which are much higher than intrinsic

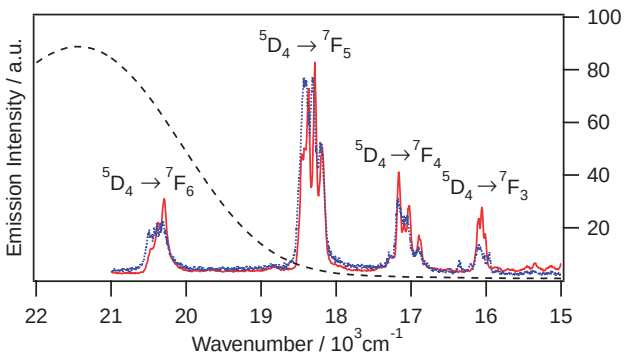

Fig. 1. Absorption spectrum of $[Co(en)_3]^{3+}$ in aqueous solution (black dashed line) and emission spectra of Δ-$[Co(en)_3]$·*rac*-$[Tb(dpa)_3]$ (blue dotted line) Δ-$[Co(en)_3]$·*rac*-$[Tb(dpa)_3]$ (red solid line) crystals at room temperature. Excitation wavelength is 337 nm (N_2 laser).

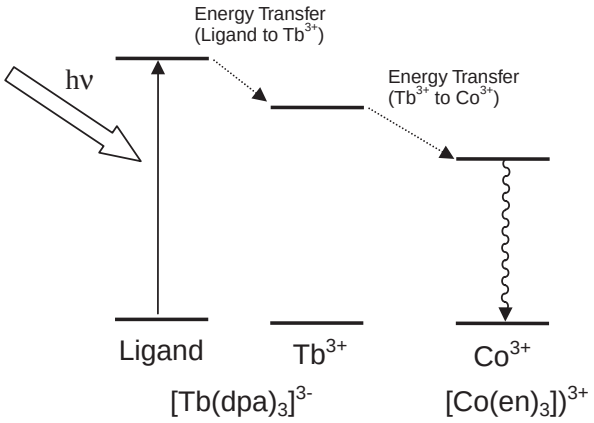

Scheme 1.

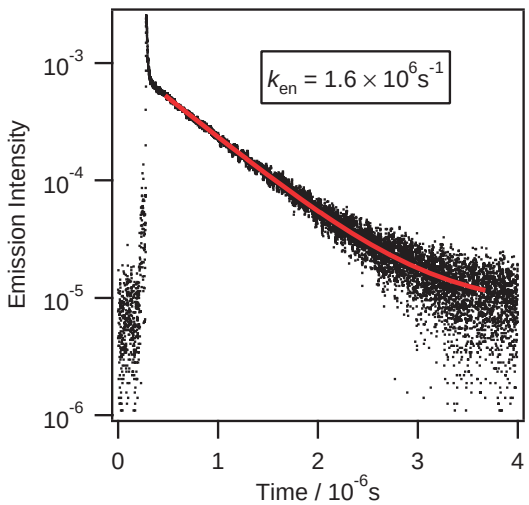

Fig. 2. Time-resolved emission intensity of *rac*-[Tb(dpa)$_3$]–*rac*-[Co(en)$_3$] crystal. Excitation wavelength is 337 nm (N_2 laser) and monitored at 546 nm at room temperature.

decay rate of $[Tb(dpa)_3]^{3-}$ luminescence. The decay rate of $K_3[Tb(dpa)_3]\cdot 3H_2O$ powder is $7.2 \times 10^3\ s^{-1}$ at room temperature. The much higher decay rate of the emission of Tb^{3+} ion means that the main relaxation path from excited Tb^{3+} is energy transfer to the Co^{III} complex, as shown in Scheme 1.

Tb–Co ET dominates the kinetics of excited Tb^{3+} in the crystals. Figure 2 shows the time profile of emission intensity monitored at 18300 cm^{-1} for single crystal of *rac*-[Co(en)$_3$]·*rac*-[Tb(dpa)$_3$], which was immersed in water. In the 0–100 μs region, the profile could be fitted with a single-exponential curve, which indicates that there is one emitting species in the crystal. Rate constant of Tb–Co ET in the crystal was determined to be $1.6 \times 10^6\ s^{-1}$. Single-exponential emission decay constants of well dried powder of *rac*-[Tb(dpa)$_3$]·*rac*-[Co(en)$_3$] was $2.3 \times 10^6\ s^{-1}$, which is larger than that of the sample immersed in water.

In contrast to the *rac*-[Co(en)$_3$]·*rac*-[Tb(dpa)$_3$] crystal, emission time profile of Δ-[Co(en)$_3$]·*rac*-[Tb(dpa)$_3$] were found to be a double-exponential decay curve. Figure 3 shows the time profile of emission intensity of single crystals of Δ-[Co(en)$_3$]·*rac*-[Tb(dpa)$_3$] monitored at 18300 cm^{-1}. The de-

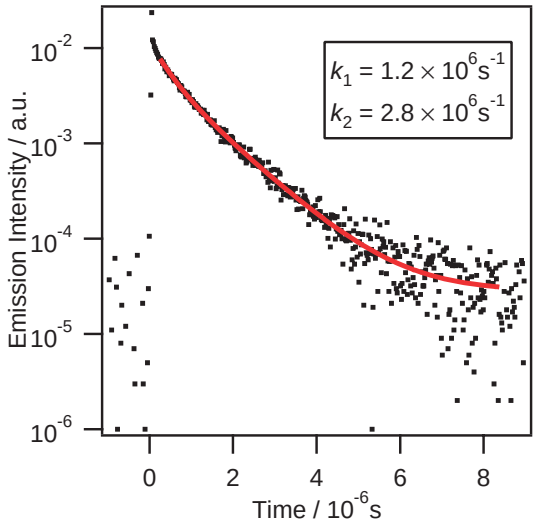

Fig. 3. Time-resolved emission intensity of *rac*-[Tb(dpa)$_3$]–Δ-[Co(en)$_3$] crystal. Excitation wavelength is 337 nm (N_2 laser) and monitored at 546 nm at 10 K.

Table 1. Decay Rate Constants of the Photo-Excited Crystals[a)]

Sample	Decay rate (Intensity) /$10^6\ s^{-1}$ (a.u.)
$K_3[Tb(dpa)_3]$	0.00072
Δ-[Co(en)$_3$]·*rac*-[Tb(dpa)$_3$]	1.2 (13600)[b)]
	2.8 (14700)[b)]
rac-[Co(en)$_3$]·*rac*-[Tb(dpa)$_3$] (wet)	1.6
rac-[Co(en)$_3$]·*rac*-[Tb(dpa)$_3$] (dry)	2.3

a) All samples were excited with a N_2 laser (337 nm) and monitored at 546 nm. b) The values in parentheses are the amplitudes for the two components of the non-exponential decay.

cay curves obtained form Δ-[Co(en)$_3$]·*rac*-[Tb(dpa)$_3$] emission were fitted with following double-exponential equation:

$$I(t) = I_1 \exp(-k_1 t) + I_2 \exp(-k_2 t), \quad (1)$$

where $I(t)$ denotes the emission intensity as a function of time (t). I_1 and I_2 are initial value of the emission intensity for each component. From the fitting, almost the same value for I_1 and I_2 were obtained, (relative intensity of I_1 and I_2, (I_1/I_2) is 0.92) and the values of k_1 and k_2 were $1.2 \times 10^6\ s^{-1}$ and $2.8 \times 10^6\ s^{-1}$, respectively. Obtaining two decay constants indicates that there are two emission species in the crystal, and the identical pre-exponential factors indicate initial populations of the two excited species are identical. The obtained decay rate constants are summarized in Table 1.

As a conclusion of this section, aspects of Tb–Co ET kinetics of Tb^{3+} in *rac*-[Co(en)$_3$]·*rac*-[Tb(dpa)$_3$] and Δ-[Co(en)$_3$]·*rac*-[Tb(dpa)$_3$] single crystals were different from each other, though emission and absorption spectra were the same. It must be due to the difference in their crystal structure, because Tb–Co ET rate constant depends on interatomic distances between Tb and Co in the crystals. Thus, we discuss the results of X-ray crystal structure analysis of *rac*-[Co(en)$_3$]·*rac*-[Tb(dpa)$_3$] and

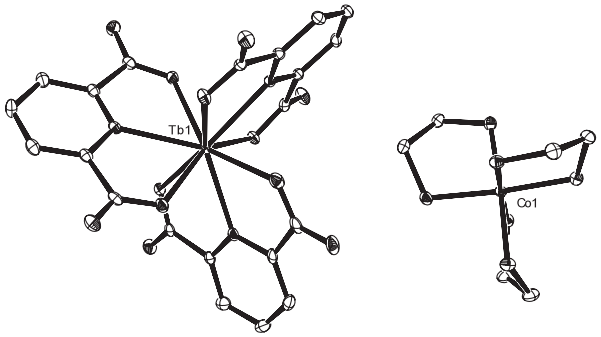

Fig. 4. ORTEP view of the asymmetric unit of *rac*-$[Co(en)_3]$·*rac*-$[Tb(dpa)_3]$. Solvent molecules and H atoms are omitted for clarify.

Table 2. Crystallographic Data

	rac-$[Co(en)_3]$·*rac*-$[Tb(dpa)_3]$	Δ-$[Co(en)_3]$·*rac*-$[Tb(dpa)_3]$
Mol. wt	1028.58	1994.93
Formula	$C_{27}H_{33}CoN_9O_{19.5}Tb$	$C_{54}H_{66}Co_2N_{18}O_{37}Tb_2$
Space group	$C2/c$	$P2_1$
Z	8	2
Cell length		
a/Å	33.05(3)	10.543(2)
b/Å	10.482(8)	21.435(3)
c/Å	23.01(2)	16.914(1)
Cell angle		
α/°	90	90
β/°	108.518(2)	95.877(9)
γ/°	90	90
V/Å^3	7559.5(99)	3802.3(7)
No. of indep reflcns	8502	11926
Max θ	27.5	14.9
R	0.0280	0.0513
R_w	0.0620	0.1107
T/K	93.1	296.2
λ/Å	0.7107	0.7107

Δ-$[Co(en)_3]$·*rac*-$[Tb(dpa)_3]$ in the next section. Two site of $[Tb(dpa)_3]^{3-}$ in Δ-$[Co(en)_3]$·*rac*-$[Tb(dpa)_3]$ in the crystal will be shown from the view point of the Tb–Co distance.

Crystal Structures of *rac*-$[Co(en)_3]$·*rac*-$[Tb(dpa)_3]$ and Δ-$[Co(en)_3]$·*rac*-$[Tb(dpa)_3]$. ***rac*-$[Co(en)_3]$·*rac*-$[Tb(dpa)_3]$:** The crystal structure of *rac*-$[Co(en)_3]$·*rac*-$[Tb(dpa)_3]$ was determined from single-crystal X-ray analysis at 93.1 K to prevent from loss of water of crystallization. An ORTEP view of asymmetric unit is shown in Fig. 4. It had seven water molecules, whose hydrogen atoms could not be determined. Crystallographic data is summarized in Table 2. Since it crystallized in the monoclinic space group $C2/c$, which has an inversion center, the asymmetric unit contained one Δ/Λ-$[Tb(dpa)_3]^{3-}$ and one Λ/Δ-$[Co(en)_3]^{3+}$ ion. $[Tb(dpa)_3]^{3-}$ was coordinated by three tridentate dpa ligands with C_3 symmetry. The Tb–O bond lengths ranged from 2.401(2) to 2.430(2) Å, and the Tb–N bond length from 2.487(2) to 2.518(2) Å.[11] As expected in the emission decay measurements, all chemical environments around Tb center of $[Tb(dpa)_3]^{3-}$ in the crystal were identical. The atomic distances between Tb–Co metal centers in Δ-$[Tb(dpa)_3]^{3-}$ and Λ-$[Tb(dpa)_3]^{3-}$, which are also identical in *rac*-$[Tb(dpa)_3]$·*rac*-$[Co(en)_3]$ crystal, are summarized in Table 3 from nearest one to the eleventh one. Nearest interatomic Tb–Co distance are not so different between homo pairs (e.g., Δ-$[Tb(dpa)_3]^{3-}$–Δ-$[Co(en)_3]^{3+}$) and hetero pairs (e.g., Δ-$[Tb(dpa)_3]^{3-}$–Λ-$[Co(en)_3]^{3+}$).

Table 3. Tb–Co Distance in $[Co(en)_3][Tb(dpa)_3]$ Crystal

	Tb–Co distance in (*rac*)$[Tb(dpa)_3]$–Δ$[Co(en)_3]$ /pm		Tb–Co distance in *rac*-$[Tb(dpa)_3]$–*rac*-$[Co(en)_3]$ /pm
	Δ-$[Tb(dpa)_3]^{3-}$	Λ-$[Tb(dpa)_3]^{3-}$	
R_1	685	564	610
R_2	686	584	617
R_3	733	801	796
R_4	749	940	969
R_5	1063	1022	1000
R_6	1112	1040	1033
R_7	1192	1171	1053
R_8	1205	1178	1149
R_9	1266	1232	1230
R_{10}	1276	1311	1278
R_{11}	1304	1333	1392

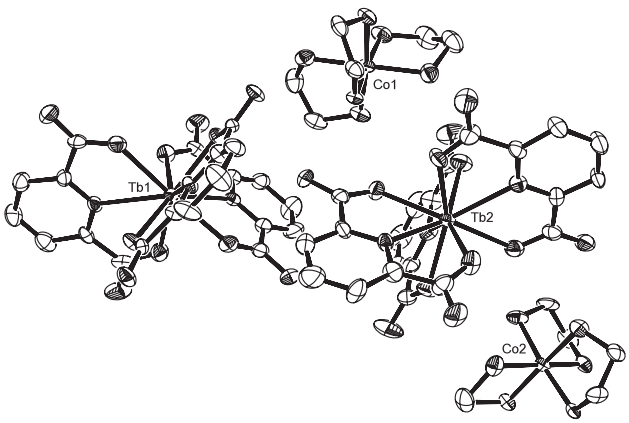

Fig. 5. ORTEP view of asymmetric unit of Δ-$[Co(en)_3]$·*rac*-$[Tb(dpa)_3]$. Solvent molecules and H atoms are omitted.

Δ-$[Co(en)_3]$·*rac*-$[Tb(dpa)_3]$: The crystal structure of Δ-$[Co(en)_3]$·*rac*-$[Tb(dpa)_3]$ was determined from single-crystal X-ray analysis at 296 K. Figure 5 shows a view of molecular coordination of Δ-$[Tb(dpa)_3]^{3-}$, Λ-$[Tb(dpa)_3]^{3-}$, and Δ-$[Co(en)_3]^{3+}$ in the crystal structure. It contained twelve water molecules, of which the hydrogen atoms could not be determined. It crystallized in the monoclinic space group $P2_1$, which has no inversion center. The absolute configuration was determined by Flack parameter. Since each asymmetric unit includes one Δ-$[Tb(dpa)_3]^{3-}$, Λ-$[Tb(dpa)_3]^{3-}$, and two Δ-$[Co(en)_3]^{3+}$ ions, there are two kinds of chemical environments around $[Tb(dpa)_3]^{3-}$ in the crystal, i.e., Δ-$[Tb(dpa)_3]^{3-}$ and Λ-$[Tb(dpa)_3]^{3-}$ are in different chemical environments from each other. The coordination sphere in each unit is similar to that in *rac*-$[Co(en)_3]$·*rac*-$[Tb(dpa)_3]$ though the bond

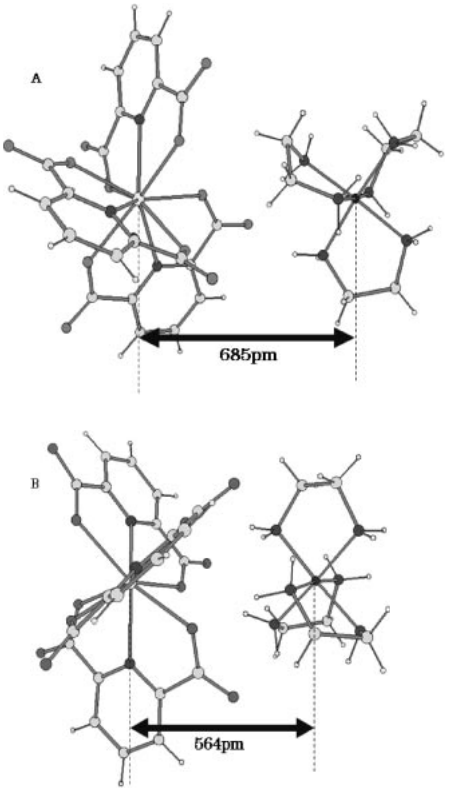

Fig. 6. Structures view of most close $[Tb(dpa)_3]^{3-}$ and $[Co(en)_3]^{3+}$ pairs in crystal of Δ-$[Co(en)_3]\cdot$*rac*-$[Tb(dpa)_3]$ estimated from single-crystal X-ray analysis. A: Δ-$[Tb(dpa)_3]$–Δ-$[Co(en)_3]$, B: Λ-$[Tb(dpa)_3]$–Δ-$[Co(en)_3]$.

lengths between Tb ion and each donor atom are slightly longer. Distances between Tb^{3+} and Co^{3+} are different between Δ/Λ-$[Tb(dpa)_3]^{3-}$. Figures 6A and 6B show views of relative positions of most close Tb–Co pairs in the crystal. Values of the closest distance from Tb to Co metal centers were 685 pm for Δ-$[Tb(dpa)_3]$ (Fig. 6A), and 564 pm for Λ-$[Tb(dpa)_3]$ (Fig. 6B). The atomic distances between Tb–Co metal centers in Δ-$[Co(en)_3]\cdot$*rac*-$[Tb(dpa)_3]$ crystal are summarized in Table 3 for Δ- and Λ-$[Tb(dpa)_3]^{3-}$. All Co atoms are in almost identical chemical environments from the viewpoint of Tb–Co atomic distance.

Brayshaw et al. have reported the splitting of $^7F_1$ level of Eu^{3+} in the crystals $[MN_6][Eu(dpa)_3]$ ($[MN_6] = [Cr(en)_3]$, $[Co(en)_3]$, and $[Co(NH)_2sar]$).[11] They have pointed out the probability of the presence of two site of Eu^{3+} in $[Co(en)_3]$-$[Eu(dpa)_3]$ from the splitting of $^5D_0$–$^7F_1$ transition (large fwhm of 2.5 cm^{-1}). Actually, in present case, there are two site in the crystal of Δ-$[Co(en)_3]\cdot$*rac*-$[Tb(dpa)_3]$, and is only one site in *rac*-$[Co(en)_3]\cdot$*rac*-$[Tb(dpa)_3]$. Thus, splitting of $^5D_0$–$^7F_0$ transition induced by diastereoisomeric difference in $[Co(en)_3][Eu(dpa)_3]$ can be detected by comparison of energy levels of *rac*- and Δ-$[Co(en)_3]\cdot$*rac*-$[Eu(dpa)_3]$, though there are still doubt for identity between crystal structures of $[Co(en)_3][Tb(dpa)_3]$ and $[Co(en)_3][Eu(dpa)_3]$.[13] A difference in the $^5D_4$–$^7F_0$ transition between *rac*- and Δ-$[Co(en)_3]\cdot$*rac*-$[Tb(dpa)_3]$ was not found, indicating that diastereoisomeric difference did not induce the splitting of the transition of Tb^{3+}.

Observation of the Kinetic Process. Intrinsic decay rate of excited Tb^{3+} can be affected by coordination water, but energy transfer to Co is drastically faster than it (more than 10^3 times). Therefore, observed excited decay rates of Tb^{3+} in $[Co(en)_3][Tb(dpa)_3]$ crystals are only determined by the Tb–Co ET process. However, there may be other factors which affect the excited state of Tb^{3+}.

Brayshaw et al. have reported that excited Tb^{3+} in Δ-$[Cr(en)_3][Tb(dpa)_3]$ decays with single-exponential curve. It is expected that crystal structure of Δ-$[Cr(en)_3][Tb(dpa)_3]$ is different from that of Δ-$[Co(en)_3]\cdot$*rac*-$[Tb(dpa)_3]$,[11] although it is ambiguous because there is no report of crystal structure of Δ-$[Cr(en)_3][Tb(dpa)_3]$. Another reason for this is an effect of the population of the excited Cr^{3+} ion, because lifetime of ^2E of $[Cr(en)_3]^{3+}$ are long enough at low temperature. However, in present case of Δ-$[Co(en)_3]\cdot$*rac*-$[Tb(dpa)_3]$, excited $[Co(en)_3]^{3+}$ are quickly decayed to ground state thermally, because emission from $[Co(en)_3]^{3+}$ were not detected. Thus, excited state of $[Co(en)_3]^{3+}$ does not affect the excited dynamics of $[Tb(dpa)_3]^{3-}$.

In rigid media, energy migrations often affect the dynamics of the excited states. In this case, one must examine the effects of energy transfer between Tb–Tb. However, Tb–Tb interaction in $[Co(en)_3][Tb(dpa)_3]$ double metal complexes crystal are expected to be so small that the energy migration is negligible in the time scale of microsecond the order, because Tb–Tb distances (about 10 Å) in the complexes are longer than Tb–Co distance (about 6 Å). Furthermore, it is known that emission of $^5D_4 \rightarrow {}^7F_6$ of Tb^{3+} metal complex crystals are stoichiometric phosphors, i.e. its decay rate does not depend on concentration of Tb^{3+} in a crystal.[12] Energy migration is ruled out if the excited kinetics in neat crystals and doped crystals are identical.[9] To estimate the Tb–Tb interaction in the crystal, time-resolved emission of doped samples of double metal complexes crystals $[Tb_xGd_{1-x}(dpa)_3]$–$[Co(en)_3]$ (x = 0.01–0.1) were performed. However, kinetic constants could not be determined because of their weak emission intensities.

It is concluded that the observed emission dynamics of the excited Tb^{3+} is dominated by the Tb–Co ET.

Temperature Dependence of Tb–Co ET Rate. Some of energy-transfer rate constants in double complex salts depend on the temperature. However, temperature dependences of the Tb–Co ET rates are small, indicating that the energy-transfer processes are a direct resonance energy transfer from Tb to Co. Figure 7 shows temperature dependence of k_1 and k_2 of Δ-$[Co(en)_3]\cdot$*rac*-$[Tb(dpa)_3]$ in the temperature region of 10–300 K. The activation energies for k_1 and k_2 obtained from the Arrhenius plots are less than 15 J mol^{-1}. Temperature dependence of energy-transfer rate in the *rac*-$[Co(en)_3]\cdot$*rac*-$[Tb(dpa)_3]$ cannot be obtained because single crystal of *rac*-$[Co(en)_3]\cdot$*rac*-$[Tb(dpa)_3]$ decompose in vacuum.

Distance and Relative Orientation Dependence. Now, it was concluded that the observed decay kinetic constants are due to direct energy-transfer rate constants from excited Tb to Co atom, and differences among three Tb–Co ET rate constants obtained from *rac*-$[Co(en)_3]\cdot$*rac*-$[Tb(dpa)_3]$ and Δ-$[Co(en)_3]\cdot$*rac*-$[Tb(dpa)_3]$ are due to differences in their crystal structures, particularly Tb–Co distance and orientation. Previously, it has been reported that relative orientation of donor

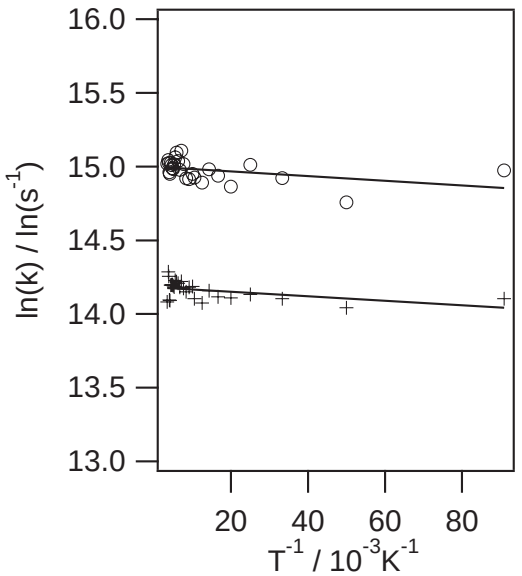

Fig. 7. Temperature dependence of energy-transfer rate constants in the crystal of $[Tb(dpa)_3]\cdot\Delta$-$[Co(en)_3]$. Cross marker denotes k_1, and circle marker k_2. E_a was estimated from the slops of the Arrhenius plots. $E_a(k_1) = 12.7$ J mol^{-1}, $E_a(k_2) = 13.1$ J mol^{-1}.

and acceptor drastically affects the Tb–Co ET rate between ^{3}MLCT state of $[Ru(N\text{-}N)_3]^{2+}$ and ^2E_g $[Cr(CN)_6]^{3-}$ in double complex crystals.[9] However, in this case, it is assumed that relative orientation dependence on the reaction is negligibly small for the energy-transfer reaction in $[Co(en)_3][Tb(dpa)_3]$ crystals to simplify the analysis. Orientation of nearest Tb–Co are not so different in Λ-$[Tb(dpa)_3]^{3-}$–$[Co(en)_3]^{3+}$ and Δ-$[Tb(dpa)_3]^{3-}$–$[Co(en)_3]^{3+}$ in the crystal of $[Tb(dpa)_3]$–*rac*-$[Co(en)_3]$. Both nearest Co^{3+} ions from Δ/Λ-$[Tb(dpa)_3]^{3-}$ have an angle of less than 15° from C_3 axis in Δ- or Λ-$[Tb(dpa)_3]^{3-}$.

Energy-Transfer Mechanism. Thus, we determined the Tb–Co ET rate constants as a function of distance between Tb–Co according to known mechanisms of the energy-transfer reaction. There are two well-known mechanisms for the energy-transfer reaction: an electron-exchange interaction and a multi pole interaction. The equation for the electron-exchange mechanism is represented by Dexter as follows:[14]

$$k_{en} = K_0 \exp\left(\frac{-2R}{L}\right) \int f_D(\tilde{\nu}) f_A(\tilde{\nu}) d\tilde{\nu}. \quad (2)$$

K_0 is pre-exponential factor that depends on the orbital interactions of reaction systems. R is distance between donor and acceptor. L is average of effective van der Waals radii of donor and acceptor species. $f_D(\tilde{\nu})$ is the normalized emission spectrum of donor, and $f_A(\tilde{\nu})$ is the normalized absorption of acceptor.

On the other hand, energy-transfer rate constant of dipole–dipole interaction mechanism is represented by the Förster equation as following:[15]

$$k_{en} = k \frac{\kappa^2 k_e}{R^6} \int f_D(\tilde{\nu}) f_A(\tilde{\nu}) \frac{d\tilde{\nu}}{\tilde{\nu}^4}. \quad (3)$$

The term k is a fundamental constant. k_e is kinetic constant of radiative transition, and κ is parameter of orientation. In each mechanism, energy-transfer rate strongly depends on the distance between the donor and acceptor. A mechanism of energy-transfer reaction involving rare-earth ions is often represented by dipole–dipole or dipole–quadrupole mechanism.[16] Furthermore, Hauser's group, who have studied energy transfer in double complex salts of $[M(bpy)_3]^{2+/3+}$ (M = Ru^{2+}, Os^{2+}, and Cr^{3+}) and $[Cr(ox)_3]^{3+}$,[10] have indicated that both super exchange mechanism and dipole–dipole mechanism are important for the energy-transfer reactions. However, in the present case, we analyzed the results of the Tb–Co ET rate constants according to the electron-exchange mechanism because of the three following reasons. First, the distances between donor and acceptor are very small (about 5 Å). Tanaka and Ishibashi have reported that Dexter mechanism by dominated in energy transfer between rare-earth ions with very close D–A distance (around 5 Å).[17] Second, as Metcalf et al. have described previously, the dipole moment of the d–d transition of Co^{3+} is very small, and the energy-transfer mechanism of electron exchange is more reasonable than the dipole–dipole interaction mechanism for the Tb–Co ET.[4] Third, the best fit to the data for the Tb–Co ET rate constants as a function of Tb–Co distance was achieved on the basis of the Dexter equation, than the Förster equation. The details of the fitting analysis is shown in the next section.

Analysis of Energy-Transfer Rate Constants as a Function of Distance. It is assumed that difference of rate constants between k_{en} for Δ-$[Tb(dpa)_3]^{3-}$ (k_Δ) and for Λ-$[Tb(dpa)_3]^{3-}$ (k_Λ) originate from the difference in Tb–Co distances in the crystals. Therefore, the values of k_1 and k_2 correspond to those of k_Δ and k_Λ calculated as follows:

$$k_{en\Delta}{}^m = K_0 \exp\left(\frac{-2R_m^\Delta}{L}\right) \int f_{M1}(\tilde{\nu}) \varepsilon_{M2}(\tilde{\nu}) d\tilde{\nu} = K_e \exp\left(\frac{-2R_m^\Delta}{L}\right), \quad (4)$$

$$k_{en\Lambda}{}^m = K_0 \exp\left(\frac{-2R_m^\Lambda}{L}\right) \int f_{M1}(\tilde{\nu}) \varepsilon_{M2}(\tilde{\nu}) d\tilde{\nu} = K_e \exp\left(\frac{-2R_m^\Lambda}{L}\right), \quad (5)$$

$$k_1 = k_\Delta = \sum_{m=1}^{\infty} k_{en\Delta}{}^m = K_e \sum_{m=1}^{\infty} \exp\left(\frac{-2R_m^\Delta}{L}\right), \quad (6)$$

$$k_2 = k_\Lambda = \sum_{m=1}^{\infty} k_{en\Lambda}{}^m = K_e \sum_{m=1}^{\infty} \exp\left(\frac{-2R_m^\Lambda}{L}\right), \quad (7)$$

where R_m is distance Tb^{3+} and Co^{3+} numbered by m from nearest one to farer one as m increase. As mentioned above, R_m is more different between $R_m{}^\Delta$, atomic distance between Δ-$[Tb(dpa)_3]^{3-}$–Δ-$[Co(en)_3]^{3+}$, and $R_m{}^\Lambda$, between Λ-$[Tb(dpa)_3]^{3-}$–Δ-$[Co(en)_3]^{3+}$. The R_m value of R_1 is much smaller for $R_1{}^\Lambda$ than $R_1{}^\Delta$. Therefore, the slower k_1 is assigned to Tb–Co ET from Δ-$[Tb(dpa)_3]^{3-}$ to Δ-$[Co(en)_3]^{3+}$, and the faster k_2 is to Λ-$[Tb(dpa)_3]^{3-}$–Δ-$[Co(en)_3]^{3+}$, because R_1 contributes more to the sum of the exponential functions than other R_m. From the closest Co^{3+} to the eleventh separated one, sum of energy-transfer rate constants were evaluated, and for more than twelfth separated species. It was using the concentration of Co atoms in the crystals as follows:

$$K_e \sum_{m=1}^{\infty} \exp\left(\frac{-2R_m}{L}\right) \approx K_e \sum_{m=1}^{11} \exp\left(\frac{-2R_m}{L}\right) + \int_{tw}^{\infty} 4\pi C K_e \exp\left(\frac{-2R}{L}\right) R^2 dR, \quad (8)$$

where C is the concentration of Co atom in the crystal obtained from X-ray analysis. *tw* means the distance between Tb and twelfth separated Co atom. From Eq. 8 and values of k_1, k_2 for Δ-[Co(en)$_3$]·*rac*-[Tb(dpa)$_3$], we obtained the pre-exponential factor K_e (8.9×10^8 s^{-1}) and effective van der Waals radius L (1.76 Å). Using these parameters, percentages of energy transfer to the nearest pair of Co ions to the sum of energy-transfer rates were calculated to be 94.2% for Λ-[Tb(dpa)$_3$]$^{3-}$ and 63.2% for Δ-[Tb(dpa)$_3$]$^{3-}$. The ratio of excited energy transfer from Tb^{3+} to the four [Co(en)$_3$]$^{3+}$ ions put in R_1 to R_4 is 99%, which indicates that after the 11th term in the integral in Eq. 8 is ignorable.

Now, for *rac*-[Co(en)$_3$]·*rac*-[Tb(dpa)$_3$], values of R_m were also obtained from X-ray crystal structure (Table 2). The calculated value of k_{en} for *rac*-[Co(en)$_3$]·*rac*-[Tb(dpa)$_3$] from Eq. 2 obtained using K_e, L, and R_m was 1.8×10^6 s^{-1}, which is close to measured value of 1.6×10^6 s^{-1}.

The ratio between k_1 and k_2 for Δ-[Co(en)$_3$]·*rac*-[Tb(dpa)$_3$] was not consistant with that of energy-transfer rates calculated from the Förster equation (Eq. 3) with the distances obtained from the result of X-ray analysis. In fact, ratio between k_1 and k_2 was more than 20% different from that calculated from the Förster's equation.

Estimation of Inter-Atomic Distance between Tb–Co in Aqueous Solutions. Previously, we have reported that the energy-transfer reactions between [Tb(dpa)$_3$]$^{3-}$ and Co^{III} complexes depend on the coexisting ions.[8] In other words, transfer rate constants of [Tb(dpa)$_3$]$^{3-}$–[Co(en)$_3$]$^{3+}$ can be changed by choosing coexisting anions. For example, the energy-transfer rate constants of [Tb(dpa)$_3$]$^{3-}$–[Co(en)$_3$]$^{3+}$ in encounter complexes were evaluated to be 1.60×10^6 s^{-1} in a 1.0 mol dm^{-3} NaCl aqueous solution and 2.7×10^7 s^{-1} in $NaClO_4$. It has been proposed that distance between donor and acceptor in encounter complexes is affected by coexisting ions due to ion association properties of [Co(en)$_3$]$^{3+}$.[18] The results of coexisting salts effects for energy-transfer reactions had been reported,[5–8] and many intermolecular chemical reactions in electrolyte are affected by such a salt effect mechanism. Thus, to estimate the distance change induced by coexisting ions in aqueous solution is very important. Thus, we tried to estimate the distances between [Tb(dpa)$_3$]$^{3-}$–[Co(en)$_3$]$^{3+}$ in the encounter complex in aqueous solutions for in the presence of Cl^- and ClO_4^- from the distance dependence of energy-transfer rate in this study. It must be noted that the value of the energy-transfer rates in the crystals of [Tb(dpa)$_3$]$^{3-}$–[Co(en)$_3$]$^{3+}$ are comparable to the estimated values of the energy-transfer rate constants in encounter complexes in solution ($k_{en} \approx 1.6$–2.7×10^6 s^{-1} in solution, $k_{en} \approx 1.2$–2.8×10^6 s^{-1} in crystal).

The distance between Tb and Co in encounter complexes of [Tb(dpa)$_3$]$^{3-}$–[Co(en)$_3$]$^{3+}$ in aqueous solutions were estimated from Dexter's equation using the values of K_e and L considering the distance dependence of diffusion step as follows:[19,20] 6.20 Å in a NaCl solution and 5.96 Å in a $NaClO_4$ solution. They are close to distance between Tb–Co in the crystals.

By assuming the relative orientation dependence was negligible, k_{en} as a function of R for [Tb(dpa)$_3$]$^{3-}$–[Co(en)$_3$]$^{3+}$ was obtained according to electron-exchange mechanism as following simple equation:

$$k_{en} = K \exp\left(\frac{-2R}{L}\right), \quad (9)$$

where $K = 8.9 \times 10^8$ s^{-1} and $L = 1.76$ Å, in the case of energy transfer from [Tb(dpa)$_3$]$^{3-}$ to [Co(en)$_3$]$^{3+}$.

Conclusion

Three rate constants of energy-transfer reactions from Tb^{3+} to Co^{3+} in crystals of double complex salts were evaluated on the basis of the X-ray crystal structures of Δ-[Tb(dpa)$_3$]$^{3-}$–Δ-[Co(en)$_3$]$^{3+}$, Λ-[Tb(dpa)$_3$]$^{3-}$–Δ-[Co(en)$_3$]$^{3+}$, and *rac*-[Tb(dpa)$_3$]$^{3-}$–*rac*-[Co(en)$_3$]$^{3+}$, of which absorption and emission spectral terms were quite similar. The two decay rate constants of Δ-[Co(en)$_3$]·*rac*-[Tb(dpa)$_3$] were assigned to emission from Δ-[Tb(dpa)$_3$]$^{3-}$ (slower one) and Λ-[Tb(dpa)$_3$]$^{3-}$ (faster one). It is surprising that the energy-transfer rates between Tb–Co could be evaluated from simple equation such as Eq. 9 in spite of complicated aspects of other energy-transfer systems in double metal complex crystals. From Eq. 9, the distance between Tb–Co in various media, e.g., in aqueous solution, can be determined by measuring the energy-transfer rate. However, relative orientations may have a strong effect.[9] Furthermore, the analysis was performed by only using the electron-exchange mechanism; however, a dipole interaction mechanism may affect the energy-transfer reactions.[10] Thus, more information and experimental data is needed for Tb–Co ET reactions between the Tb–Co metal complexes in a rigid phase.

The values of energy-transfer rate constants are comparable with those in fluid systems, and distances in solution were evaluated from the distance dependence obtained from the crystals. It is noted that such a small change in distance <0.2 Å, considerably affects the energy-transfer reaction in the electron-exchange mechanism.

The authors express to Prof. T. Tsubomura at Seikei University for X-ray analysis and kind discussion.

References

1 I. Fujita, H. Kobayashi, *Ber. Bunsen-Ges. Phys. Chem.* **1972**, *76*, 115.

2 F. Basolo, R. G. Pearson, *Mechanisms of Inorganic Reactions*, 2nd ed., John Wiley & Sons, Inc., **1967**.

3 G. J. Kavarnos, *Fundamentals of Photoinduced Electron Transfer*, John Wiley & Sons, Inc., New York, **1993**.

4 D. H. Metcalf, S. W. Snyder, J. N. Demas, F. S. Richardson, *J. Am. Chem. Soc.* **1990**, *112*, 5681.

5 M. Iwamura, T. Otsuka, Y. Kaizu, *Inorg. Chim. Acta* **2002**, *333*, 57.

6 M. Iwamura, T. Otsuka, Y. Kaizu, *Inorg. Chim. Acta* **2004**, *357*, 1565.

7 M. Iwamura, M. Morita, *Inorg. Chim. Acta* **2004**, *357*, 3451.

8 M. Iwamura, M. Morita, T. Otsuka, Y. Kaizu, *J. Mol. Liq.*

2006, *128*, 71.

9 T. Otsuka, A. Sekine, N. Fujigasaki, Y. Ohashi, Y. Kaizu, *Inorg. Chem.* **2001**, *40*, 3406.

10 M. E. von Arx, A. Hauser, *Phys. Rev. B* **1996**, *54*, 15800. b) V. S. Langford, M. E. von Arx, A. Hauser, *J. Phys. Chem. A* **1999**, *103*, 7161.

11 P. A. Brayshaw, J. C. G. Bunzli, P. Froidevaux, J. M. Harrowfield, Y. Kim, A. N. Sobolev, *Inorg. Chem.* **1995**, *34*, 2068.

12 J. H. Bigelow, *Inorganic Synthesis*, McGraw-Hill, New York, **1946**, Vol. II.

13 In an unpublished study, we are trying to prepare the single crystals of *rac*-$[Co(en)_3]\cdot$*rac*-$[Eu(dpa)_3]$ and Δ-$[Co(en)_3]\cdot$*rac*-$[Eu(dpa)_3]$. It is expected that crystal structures of $[Co(en)_3]$-$[Eu(dpa)_3]$ are somewhat different from $[Co(en)_3][Tb(dpa)_3]$ because crystal of Δ-$[Co(en)_3][Eu(dpa)_3]$ decompose in contrast to Δ-$[Co(en)_3]\cdot$*rac*-$[Tb(dpa)_3]$, which is rigid in air, though they were prepared with identical method.

14 D. L. Dexter, *J. Chem. Phys.* **1953**, *21*, 836.

15 T. Förster, *Discuss. Faraday Soc.* **1959**, *27*, 7.

16 S. Hüfner, *Optical Spectra of Transparent Rare Earth Compounds*, Academic Press, New York, **1978**.

17 F. Tanaka, T. Ishibashi, *J. Chem. Soc., Faraday Trans.* **1996**, *92*, 1105.

18 H. Yokoyama, T. Ohta, M. Iida, *Bull. Chem. Soc. Jpn.* **1992**, *65*, 2901.

19 R. Fuoss, *Trans. Faraday Soc.* **1934**, *30*, 967.

20 P. Debye, *Trans. Electrochem. Soc.* **1942**, *82*, 265.